ACS Sustainable Chemistry & Engineering

Research Article

pubs.acs.org/journal/ascecg

Low-Temperature Nitrogen Doping in Ammonia Solution for Production of N-Doped TiO_2-Hybridized Graphene as a Highly Efficient Photocatalyst for Water Treatment

Wen Qian,[†] P. Alex Greaney,[‡] Simon Fowler,[†] Sheng-Kuei Chiu,[§] Andrea M. Goforth,[§] and Jun Jiao*,[†]

[†]Department of Physics and Department of Mechanical and Materials Engineering, Portland State University, Portland, Oregon 97201, United States

[‡]School of Mechanical, Industrial, and Manufacturing Engineering, Oregon State University, Corvallis, Oregon 97331, United States

[§]Department of Chemistry, Portland State University, Portland, Oregon 97201, United States

Supporting Information

ABSTRACT: To facilitate the potential application of TiO_2 as an efficient photocatalyst, the modulation of its band gap and electrical structure is of great significance. Herein, we report a very simple nitrogen (N)-doping method to obtain N-doped TiO_2, which is hybridized with graphene sheets at a temperature as low as 180 °C and using an ammonia solution as the N source and reaction medium. X-ray photoelectron spectroscopy analysis revealed that the atomic N level could reach 2.4 atomic percent when the reaction time was 14 h. Photoluminescence (PL) emission spectra indicated that N-doped TiO_2/graphene composites have drastically suppressed TiO_2 PL intensity when compared to undoped TiO_2, confirming the lower recombination rate of electron−hole pairs in the N-doped TiO_2. Additionally, photodegradation data showed that the decomposition rate of methylene blue with our N-doped TiO_2/graphene photocatalyst is twice as fast as a commercial Degussa P25 catalyst. Furthermore, density functional theory (DFT) calculations demonstrate that N doping creates empty states in the band gap of the TiO_2 that are below the Fermi energy of graphene. Thus, when N-doped TiO_2 is brought into contact with graphene, these states become filled by electrons from the graphene, shifting the TiO_2 bands upward relative to the graphene. Such a shift in band alignment across the TiO_2/graphene heterojunction makes transfer of the photoexcited electron more energetically favorable. This work provides a very convenient chemical route to the scalable production of N-doped TiO_2/graphene photocatalyst for potential applications in wastewater treatment.

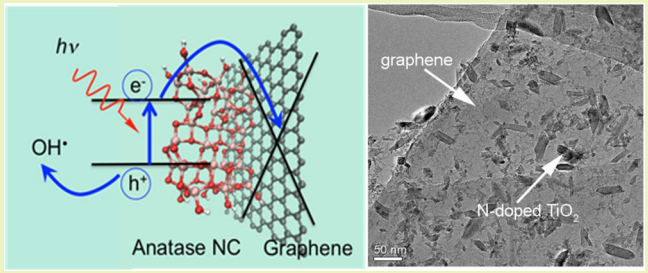

KEYWORDS: *Graphene, N-doped TiO_2, Low temperature doping, Ammonia solution, Photocatalyst, Wastewater treatment*

INTRODUCTION

The potential of TiO_2 as a photocatalyst is well recognized and has been studied extensively over many decades. In addition to being photoactive, it is chemically stable, nontoxic, and inexpensive,[1−3] making it very attractive for industrial-scale water treatment and the degradation of recalcitrant environmental pollutants. In this application, absorbed ultraviolet (UV) radiation excites electrons from the TiO_2 valence band to the conduction band, thus forming electron−hole pairs. The holes subsequently react as oxidants on surface-adsorbed hydroxide ions to produce hydroxyl free radicals, which in turn are the main oxidizing agents responsible for photo-oxidation of organic contaminants.[1] However, despite the great potential of TiO_2 for water treatment, there are two obstacles that have hampered industrial-scale adoption. The first is that TiO_2 photocatalysts are not photoactive under visible light; the second is the fast recombination rate of electron−hole pairs, which results in the low efficiency of competing photoinduced chemical reactions.

During the past decades, N doping has been proven to be the most effective strategy for altering the electronic structure of TiO_2, enabling the response of photocatalytic activity in the visible light region. To date, many experimental approaches have been developed to produce N-doped TiO_2 with visible light sensitivity, including sputtering,[4,5] thermal nitridation of TiO_2,[6] direct amination,[7] and pulsed laser deposition.[8] All these N-doping procedures were carried out at high temperatures (>400 °C) or required complicated and expensive equipment. However, based on the density functional theory (DFT) calculations by Tsetseris,[9] high temperatures may not be required if N dopants are introduced to anatase TiO_2 interstitially (N_i) rather than substitutionally (N_s) because the diffusion of N to N_i sites becomes operative at much lower temperatures (100−300 °C). Inspired by such theoretical results, in this work, we have developed a novel low-

Received: February 20, 2014
Revised: May 21, 2014
Published: June 13, 2014

   dx.doi.org/10.1021/sc5001176 | ACS Sustainable Chem. Eng. 2014, 2, 1802−1810

temperature (180 °C) doping process to synthesize N-doped TiO_2 hybridized graphene using a liquid ammonia solution as the nitrogen source. While the N doping alters the band gap to allow visible light absorption, the synergistic anchoring of the N-doped TiO_2 nanoparticles to graphene decreases the rate of electron−hole pair recombination and increases the rate of photo-oxidation, as described below. To our knowledge, no comparable low-temperature methodology for the preparation of N-doped TiO_2/graphene composites has been reported before.

It is well recognized that graphene acts as an electron acceptor due to its 2D $\pi-\pi$ conjugation, which may decrease the radiative recombination rate and increase the catalytic activity of nanoparticle photocatalysts anchored to the graphene surface. Taking advantage of the high electron mobility of graphene (2×10^5 cm^2/V s),[10] if the TiO_2/graphene interface is clean, the excited electrons of TiO_2 will transfer quickly from the conduction band of TiO_2 to graphene and, therefore, greatly delay the electron−hole recombination. Also, due to a high surface area (2600 m^2/g),[11] graphene sheets will not only allow the TiO_2 nanocrystals (NCs) to be well dispersed on the surface but also facilitate attachment of aromatic organic contaminants in treated water solution because graphene is hydrophobic and lipophilic in water and can act as a selective adsorbent.[12] Overall, the combination of exfoliated crystalline graphene and N-doped TiO_2 is expected to simultaneously improve the performance of TiO_2 as a photocatalyst by (1) extending photosensitivity to the visible light range, (2) decreasing carrier recombination rates by increasing electron−hole separation, and (3) increasing pollutant degradation rates through favorable absorption of organic pollutants.

Recognizing the advantages of graphene-hybridized TiO_2, the initial report by Zhang et al. used a hydrothermal reaction to hybridize graphene oxide (GO) with commercial Degussa P25;[13] afterward, a number of similar studies were reported.[14−25] Their experimental results suggest that graphene−TiO_2 composites have a better photocatalytic performance in comparison to TiO_2 catalysts alone. Although these results are promising, the use of GO as a precursor for the preparation of graphene−TiO_2 composites poses a significant disadvantage because there exists a high density of defects in the lattices of GO, leading to the severe disruption of graphene's intrinsic electronic transport property. To overcome this challenge, we selected and prepared highly crystalline graphene as a substrate instead of using GO. During the past two years, we have developed the "thermal expansion−liquid exfoliation−solvothermal reaction (TELESR)" process to hybridize high-quality exfoliated graphene with various transition metal (Fe, Mn, Co) oxides[26] and noble metal (Pt, Pd, and Pt-based alloys) nanoparticles.[27,28] We have demonstrated the advantage of using the high-quality conductive graphene prepared in this way as a platform for anchoring nanoparticles to fabricate hybridized nanoparticle/graphene composites with superior properties.

In the present study, we used this TELESR process to successfully hybridize graphene with N-doped TiO_2 NCs at a low temperature of 180 °C for the purpose of overcoming the two main obstacles mentioned above. This was done using titanium(IV) butoxide and exfoliated graphene as precursors and an ammonia solution in isopropanol (IPA) as both the solvent and nitrogen source. Photodegradation testing demonstrated that graphene-supported N-doped TiO_2 showed significant improvement for decomposing a representative dye, methylene blue (MB), when compared to both commercial Degussa P25 and the undoped TiO_2 prepared under the same conditions. Additionally, we have performed electronic structure calculations that provide mechanistic understanding of the synergy between N-doped TiO_2 and the graphene substrate. The simple and low-temperature nitrogen-doping method via a liquid ammonia solution to produce a N-doped TiO_2/graphene composite, which we have demonstrated here, could make large-scale production of these materials both economical and sustainable, finally unlocking the potential of TiO_2 as an efficient photocatalyst for wastewater treatment.

EXPERIMENTAL AND SIMULATION METHODS

Chemicals and Materials. 1-Methyl-2-pyrrolidone (NMP), anhydrous, 99.5%, Sigma-Aldrich; anhydrous isopropanol (IPA), 99.5%, Sigma-Aldrich; titanium(IV) butoxide, $Ti(OBu)_4$, 99.5%, Sigma-Aldrich; ammonia solution (2M) in IPA, Sigma-Aldrich. All of them were purchased and used as received. Commercially available expandable graphite (average diameter 300 μm, 99% purity, Beijing Invention Biology Engineering & New Material Co., Ltd., China) was exfoliated as described below. Photodegradation performance was evaluated relative to commercially available AEROXIDE TiO_2 P25 (Evonik Degussa).

Thermal Expansion and Liquid Exfoliation Process To Obtain Few-Layer Graphene. In a typical synthesis, commercially available expandable graphite was rapidly heated to 1000 °C and maintained for 60 s under the atmosphere of forming gas (5% H_2 and 95% Ar). The resulting expanded graphite (EG) was mixed with NMP. The few-layer graphene sheets were then exfoliated from the EG through durative sonication for 60 min (Misonix Sonicator 3000, 700 W power), followed by centrifugation at 300 rpm (900 g) for 30 min, forming a sustainable gray suspension. Finally, the solid exfoliated pristine graphene sheets were collected by centrifugation at 15,000 rpm for 3 min and separated without any heat treatment, surface modification, or oxidation process, as shown in Figure S1 of the Supporting Information.

Production of Reduced Graphene Oxide. Graphene oxide was prepared from natural graphite powder by a modified Hummer's method.[29,30] Graphite powder (1 g), $NaNO_3$ (0.5 g), and 23 mL of concentrated sulfuric acid were added into a 250 mL round-bottomed flask and stirred at room temperature for 24 h. Next, the flask was moved into an ice bath, and 3 g of $KMnO_4$ was slowly added under vigorous agitation. The flask was then heated in a water bath at 38 °C for 2 h. A total of 46 mL of water was gradually added to the flask, and the suspension was allowed to stir for 15 min. The suspension was diluted by 140 mL of water, and the reaction was ended by addition of 10 mL of 30% H_2O_2. Ten minutes later, the bright yellow suspension was centrifuged and washed with 10% HCl solution twice. The precipitate was finally washed with DI water, collected by centrifugation, and dried in a vacuum oven at 70 °C overnight. Reduced graphene oxide (RGO) was then produced using hydrazine hydrate as a reducer.[31] Briefly, 100 mg of the graphene oxide was dispersed in 100 mL of DI water, stirred for 30 min, and then 1.0 mL of $N_2H_4{\cdot}H_2O$ was added. The mixtures were heated at 95 °C using a water bath for 45 min, forming a black solid precipitate, and then finally were isolated by filtration and washed with DI water.

Solvothermal Reaction to Deposit N-doped TiO_2 NCs onto the Few-Layer Graphene Surface. The resulting few-layer graphene stacks (5 mg), $Ti(OBu)_4$ (0.02 g, 0.05 mmol), and ammonia solution (2M) in IPA (20 mL) were mixed and mechanically stirred for 30 min. The mixture was then transferred to a closed stainless-steel autoclave with a Teflon liner (25 mL in total capacity). The autoclave was heated to 180 °C and maintained at this temperature for time periods ranging from 7 to 21 h. Similarly, for producing an undoped TiO_2/graphene composite (as shown in Figure S2, Supporting Information), as well as for producing an undoped TiO_2/RGO composite, the precursors and reaction conditions were almost the

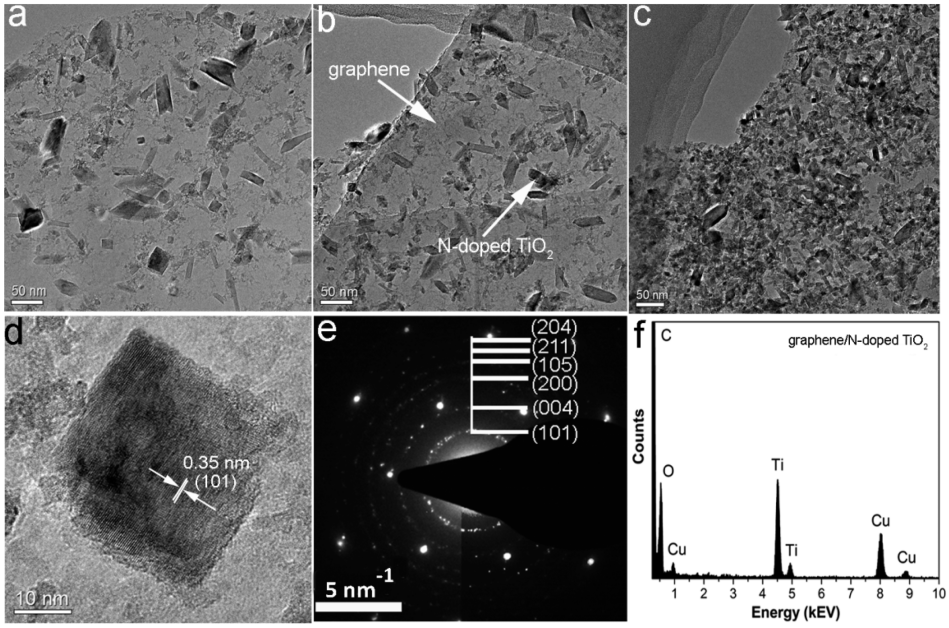

Figure 1. TEM analysis of N-doped TiO_2/graphene prepared at a low temperature of 180° at varying reaction times of 7 h (a), 14 h (b), and 21 h (c). (d) HRTEM image of deposited N-doped TiO_2 NCs. (e) Corresponding SAED pattern. (f) Typical EDX pattern of deposited N-doped TiO_2 NCs.

same, except that IPA was used as the solvent instead of an ammonia solution of IPA. Because the precursor amount of graphene and titanium are the same for producing the N-doped TiO_2/graphene, undoped TiO_2/graphene, and undoped TiO_2/RGO, the ratio of graphene in these composites should also be the same. We calculated the addition ratio of graphene in all these composites, which is about 55.6%.

Structural and Properties Characterization. An FEI TECNAI F20 transmission electron microscope (TEM) with EDX and GIF systems, operating at an accelerating voltage of 200 kV, was used for analysis of the morphology and crystal structure of N-doped TiO_2/graphene composites. ImageJ and Digital Micrograph programs were utilized to analyze the particle size and coating density based on 24 TEM images. Specifically, we adjusted the contrast and thresholds of the image until ImageJ was able to give a percentage of black vs white pixels. Raman spectra were collected with a HORIBA Jobin Yvon LabRAM Raman spectrometer using an Ar^+ laser (532 nm). Photoluminescence spectra were acquired using a 15 mW 325 nm HeCd laser as the excitation source. Powder X-ray diffraction (XRD) studies were performed in the 20−70° 2θ range using a Rigaku Ultima IV X-ray diffraction system with graphite monochromatized Cu K_α radiation (λ = 1.54187 Å). Samples for X-ray analysis (as-prepared graphene, as-prepared N-doped TiO_2, and N-doped TiO_2/graphene composites) were dropped from ethanol and deposited as thin films on glass slides.

Photocatalytic Activity Measurements. The photocatalytic activity of N-doped TiO_2/graphene composites as well as undoped TiO_2/graphene and undoped TiO_2/RGO were evaluated by degradation of MB in an aqueous solution. Typically, 5 mg of photocatalyst was mixed with a 20 mg/L MB solution. The suspension was first stirred in the dark for 60 min to reach the adsorption−desorption equilibrium of MB dye. Afterward, the mixture was illuminated with a 150 W Xe lamp (Newport, Oriel Instrument, model 67005) under magnetic stirring. Aliquots (2.0 mL) were drawn out of the solution at 15 min intervals after the start of sample illumination. The MB solution aliquots were separated from the photocatalyst by centrifugation. The dye concentration in the supernatant was analyzed using a UV−vis-NIR 3600 spectrophotometer (Shimadzu).

Simulation Methods and Model Systems. To provide mechanistic insight into the superior photocatalytic performance of the N-doped TiO_2/graphene composites, DFT was used to compute the electronic structure of the composite and its heterojunction. Calculations were performed using the SIESTA DFT package[32] using the Wu−Cohen generalized gradient exchange−correlation functional,[33] with relativistic core-corrected pseudopotentials to treat the core electrons and an energy cutoff of 300 Ry. Atom positions were relaxed such that forces were less than 0.01 eV per Å. The nanoparticles were modeled as a small slab of TiO_2 consisting of six planes of TiO_2 in the [001] direction and three and six Ti layers in the [100] and [010] directions, respectively. The small slab contained 30 Ti and 54 O atoms, and the Ti atoms on the (001) surfaces were modeled as being passivated with OH. Such a model particle is not stoichiometric. But it is charge neutral, and its density of electronic states closely matches that of bulk anatase. The relaxed configurations and electronic structures of doped and undoped anatase particles were computed both in isolation and in contact with graphene. The graphene in these calculations was a 27.21 × 17.15 $Å^2$ rectangular patch (176 C atoms), with the long direction parallel to $[21\bar{1}0]$ periodically repeated to form an infinite sheet. The anatase was placed with its narrow (100) face contacting the graphene. It was arranged initially with a 3−4 Å spacing across the contact, and the system was fully relaxed. Several different initial configurations were used, and all resulted in the same final configuration. In these calculations, the TiO_2 formed no covalent bonds with the graphene with the particle adhering to the graphene through van der Waals interactions. As there is no evidence of preferred orientation in the anatase portion of the powder X-ray diffraction pattern (Figure S3, Supporting Information), there is evidently no any preferred plane orientation relation between the anatase particles and the graphene sheets. Thus, the model particle was oriented with the graphene patch in such a way as to minimize the number of C atoms required in the calculation, while maintaining sufficient spacing between the periodic images of the TiO_2 nanoparticle. The model N-doped TiO_2 NC was doped both substitutionally and interstitially with a single N atom, which gives a 1.1 atom % doping concentration—equivalent to the doping concentration achieved experimentally through the TELESR process in liquid ammonia solution for 7 h. Several different doping sites were tested, and each resulted in qualitatively similar results. In addition, the structure of a TiO_2 NC doped with N_i and N_s atoms simultaneously was also computed. It should be noted that DFT is well known to underestimate the electronic band gap, and thus, in these calculations, we are careful not to interpret the predicted band gap quantitatively

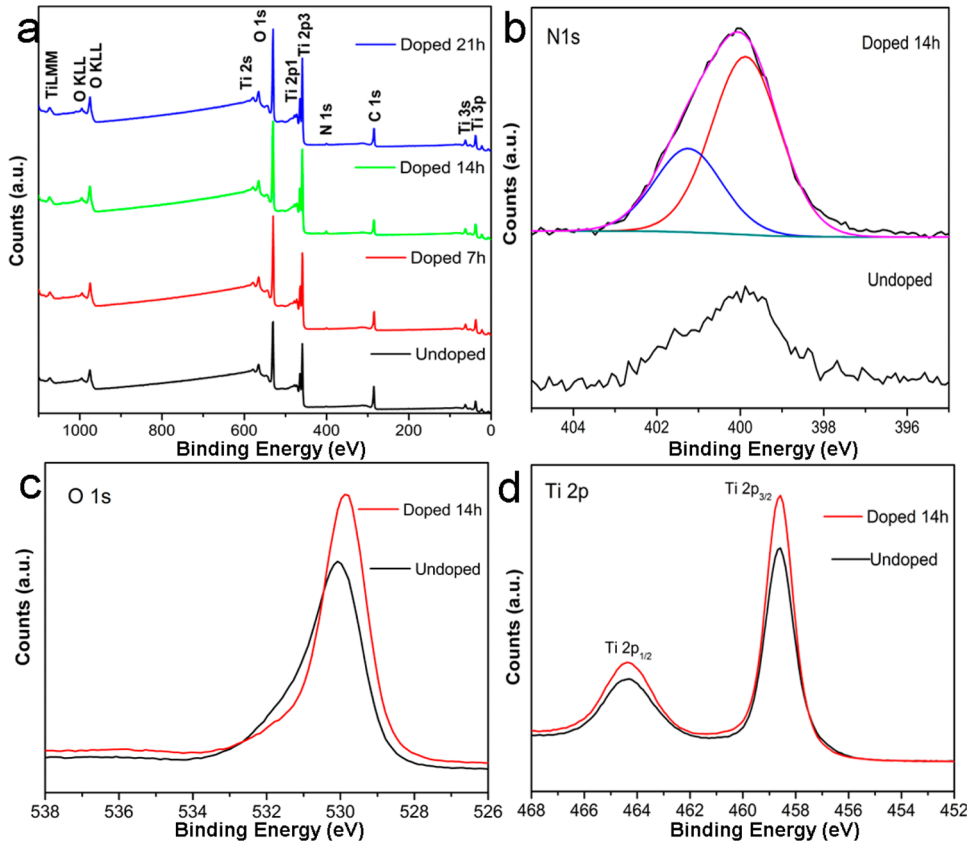

Figure 2. XPS spectra of N-doped TiO_2/graphene and undoped TiO_2/graphene hybrids. (a) XPS spectra of N-doped TiO_2/graphene hybrid prepared at 180 °C from 0–21 h, respectively. (b) Comparison of N 1s spectra between N-doped TiO_2/graphene obtained at 14 h and undoped TiO_2/graphene samples. The N 1s peak can be fitted by two Lorentzian peaks at 401.2 and 399.8 eV, which are labeled by blue and red lines, respectively. (c) Comparison of O 1s spectra between N-doped TiO_2/graphene obtained at 14 h and undoped TiO_2/graphene sample. (d) Comparison of Ti 2p spectra between N-doped TiO_2/graphene obtained at 14 h and undoped TiO_2/graphene sample.

but rather examine relative band alignment and the formation of defect states.

RESULTS AND DISCUSSIONS

Our unique reaction process (TELESR), which uses $Ti(OBu)_4$, IPA, $NH_3{\cdot}H_2O$, and exfoliated highly crystalline graphene, facilitates the low-temperature growth of N-doped TiO_2 in a gentle nitrogen-doping process, utilizing dissolved ammonia as the N source and reaction medium. TEM images (Figure 1a–c) show the N-doped TiO_2/graphene hybrids prepared in the TELESR process using reaction times of 7 h (a), 14 h (b), and 21 h (c), respectively. These images indicate that the coating density can be easily tailored by varying the reaction time. When the reaction time was 7 h, the particle coating density was only about 20%–30% of the exposed surface. As the reaction time was increased to 14 h, the particle coating density was increased to about 30%–40%. As the reaction time was further extended to 21 h, the particle coating density further increased to nearly 90%. A high resolution TEM image (Figure 1d) shows that a typical N-doped TiO_2 NC is well crystallized with a lattice spacing of 0.35 nm, which corresponds to the (101) plane of anatase TiO_2. In addition, the corresponding selected area electron diffraction (SAED) pattern (Figure 1e) exhibited not only the typical 6-fold symmetric diffraction pattern ascribed to graphene, but also multiple diffraction rings that can be indexed with anatase TiO_2 [(101), (004), (220), (105), (211) and (204), from inner to outer, respectively]. Elemental identification of the attached NCs was performed using energy-dispersive X-ray spectroscopy (EDX). The spectrum, shown in Figure 1f, revealed the presence of Ti and O in the hybrid (Cu in the spectrum was attributed to the copper TEM grid). Moreover, the XRD pattern of the N-doped TiO_2/graphene composite confirms the anatase phase of the N-doped TiO_2 nanoparticles on the graphene surfaces, and no other crystalline phases are present (as shown in Figure S3, Supporting Information).

It is interesting to note that some of the attached TiO_2 NCs in the TEM images have nanocuboid habits. Considering that anatase TiO_2 adopts a tetragonal structure with lattice parameters $a = b = 0.377$ nm and $c = 0.950$ nm, the square surface of the nanocuboid particles can be assigned as {001} facets; it has been previously shown that the (001) surface of anatase TiO_2 is the most catalytically active.[34,35] In the TELESR process, the graphene substrate may act as a morphactin, facilitating the growth of attached TiO_2 into nanocuboid shape. More systematic optimization of synthesis parameters is underway for the purpose of producing a high yield of particles with nanocubic morphology, as such a sample anchored to graphene would present more catalytically active {001} facets.

As to the possible reaction mechanism for loading N-doped TiO_2 NCs on highly crystalline graphene surfaces, we propose the following four steps of "decomposition–doping–adsorption–coalescence", analogous to the mechanism for decorating graphene with transition metal (Fe, Mn, Co) oxide NCs, as described in our previous work.[26] Briefly, first, a titanium

precursor ($Ti(OBu)_4$) is rapidly decomposed at an elevated temperature, producing some TiO_2 monomers in the presence of solvents (IPA and $NH_3{\cdot}H_2O$). Second, in the ammonia solution, oxygen vacancies are partially doped with nitrogen via atomic diffusion.[9,36] Third, due to very high surface energy, these N-doped TiO_2 seeds are preferentially adsorbed onto the graphene surface, finally coalescing into well-dispersed N-doped TiO_2 NCs. As we discussed in the Introduction, a solvothermal reaction at 180 °C can overcome diffusion barriers, enabling the diffusion of atomic N_i in anatase TiO_2.

High-resolution XPS spectra of the graphene supported N-doped TiO_2 prepared using ammonia solution as the N source with reaction times varying from 0 to 21 h confirmed the presence of various N doping levels, as shown in Figure 2a–d. The peaks at 285.1, 400.1, 530.1, 531.5, and 565.4 eV (Figure 2a) can be assigned to C 1s, N 1s, Ti 3p, O 1s, and Ti 2s, respectively. In the as-prepared TiO_2/graphene (Figure 2a, undoped), the atomic N percentage is only 0.6 atom %, while in the N-doped TiO_2/graphene (Figure 2a, doped 7–21 h), the atomic percentage of N ranges from 1.1 to 2.4 atom %, increasing at first from 7 h (1.1 atom %) to 14 h (2.4 atom %) reaction time and then decreasing from 14 to 21 h (1.3 atom %) reaction time. These results indicate that due to the dynamic equilibrium of atomic diffusion in the solution phase the concentration of N-doped atoms will first increase and then decrease as a function of reaction time,[37] reaching saturation when the reaction time is between 14 and 21 h.

The N 1s spectra of N-doped TiO_2/graphene (doped 14 h) and undoped TiO_2/graphene were compared, as shown in Figure 2b. A weak peak in the spectrum of undoped TiO_2 was observed and attributed to N_2 molecules adsorbed on the TiO_2. For the N-doped TiO_2 sample, a relatively strong peak was observed. After curve-fitting, we attributed the peak at 399.8 eV to anionic N in N–Ti–O bonds and the peak at 401.2 eV to oxidized N in Ti–O–N.[38,39] Both are due to the filling of oxygen vacancies by interstitial N atoms in the anatase lattice, which is consistent with other reports.[40,41] The XPS results support the success of the TELESR process with ammonia solution for effectively N-doping anatase TiO_2, although there was no obvious 396 eV band assignable to Ti–N bonds produced by replacement of oxygen with substitutional N atoms.[4,42,43] In addition, there is a shift of the O 1s peak by 0.3 eV toward low energy in N-doped TiO_2 (Figure 2c), indicating the existence of concomitant oxygen deficiencies,[40,44] which resulted in increased outer electron density of O and, consequently, decreased binding energy. As for the Ti 2p, the typical binding energies of Ti $2p_{3/2}$ and Ti $2p_{1/2}$ at 458.5 and 464.3 eV remain unchanged before and after doping (Figure 2d) because the amounts of doped nitrogen species were not high enough to affect their bands.

Photoluminescence (PL) emission spectra have been widely used to investigate the efficiency of charge carrier trapping, migration, and transfer, as well as to understand the fate of electron–hole pairs in semiconductors, because PL emission is highly sensitive to the abundance of surface states in the band gap.[38,45,46] Figure 3 shows the PL spectra of the undoped TiO_2/graphene and N-doped TiO_2/graphene with different atomic N percentages. All samples exhibit a broad signal from 400 to 600 nm, attributed to surface defects, such as an oxygen vacancies,[45,47,48] as well as to the recombination of carriers trapped in the localized surface states.[49,50] Compared to the undoped TiO_2/graphene, the N-doped TiO_2/graphene produced with different reaction times (7, 14, and 21h) leads to

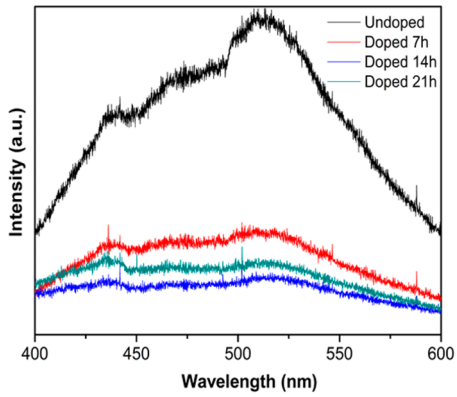

Figure 3. PL spectrum of four samples including undoped TiO_2/graphene and N-doped TiO_2/graphene prepared at different doping times at 7, 14, and 21 h, respectively.

drastic suppression of the PL signal with different efficiencies, which is probably ascribed to that the photoinduced electrons are trapped by the oxygen vacancies, and the holes are efficiently captured by the doped N_i.[38,51] Because the PL emission is the result of the recombination of excited electrons and holes, the lower PL intensity of the N-doped TiO_2/graphene samples confirms the lower recombination rates.[15,52]

Raman spectroscopy has been accepted as a versatile, purely optical, high-throughput technique for evaluating structural defects, number of layers, and doping level of graphene. Six Raman active modes for anatase TiO_2,[42,53,54] $A_{1g} + 2B_{1g} + 3E_g$, could be detected at 151 cm^{-1} (E_g), 199 cm^{-1} (E_g), 397 cm^{-1} (B_{1g}), 515 cm^{-1} (A_{1g}), 524 cm^{-1} (B_{1g}), and 639 cm^{-1} (E_g), as shown in Figure 4a, which indicates that anatase is the sole TiO_2 phase. The Raman spectrum of graphene is characterized by three main features: G, D, and 2D modes, each having different physical origins. The peak at ~1580 cm^{-1} (G band), arising from emission of zone-center optical phonons, corresponds to the doubly degenerate E_{2g} mode of graphite and is related to the coplanar vibration of sp^2-bonded carbon atoms. The peak at ~1347 cm^{-1} (D band) is related to the occurrence of defects and disorders. The peak at ~2700 cm^{-1} (2D band) originates from second-order zone boundary phonons and varies with the number of graphene layers. For the substrate of exfoliated graphene, the intensity ratio of the D to G band (I_D/I_G = 0.086) is very small, reflecting the very low defect density of graphene. Furthermore, the line shape of the 2D band can be investigated to determine the number of graphene layers.[55,56] The single 2D peak of monolayer graphene splits in four components in the bilayer graphene, $2D_{1B}$, $2D_{1A}$, $2D_{2A}$, and $2D_{2B}$. For few-layer graphene, the four components evolve into only two components by decreasing the relative intensity of the lower frequency $2D_1$ peaks. The 2D peak of a typical sample was fitted (Figure 4b), then compared with the results obtained by Graf et al.,[57] to identify the number of graphene layers as four-layer.

Furthermore, we also tested the UV–vis absorption spectra of six samples, including commercial Degussa P25, undoped TiO_2/graphene, and N-doped TiO_2/graphene prepared at different doping times of 7, 14, and 21 h, as well as N-doped TiO_2 without graphene (Figure 5). In the spectrum of the undoped sample, only absorption in the UV range (<400 nm) can be observed; but for the commercial Degussa P25 and N-doped TiO_2 with and without graphene samples, an enhanced absorption in the visible range between 400 and 600 nm can be

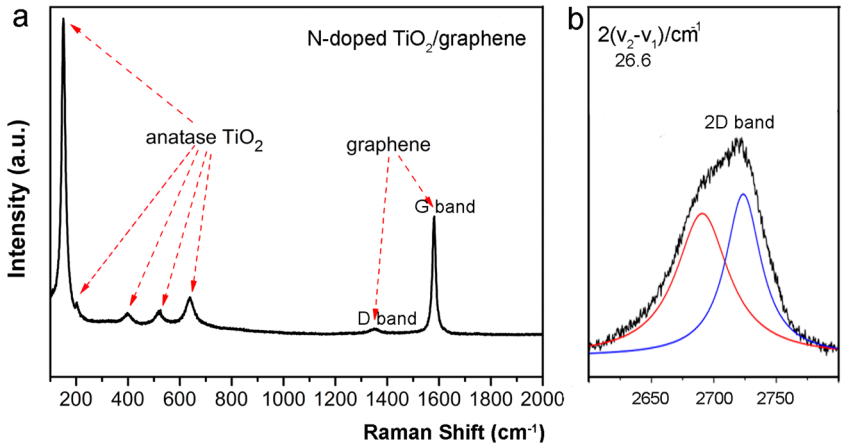

Figure 4. Raman spectrum of a N-doped TiO_2/graphene sample (a) with 2D peak fitting (b).

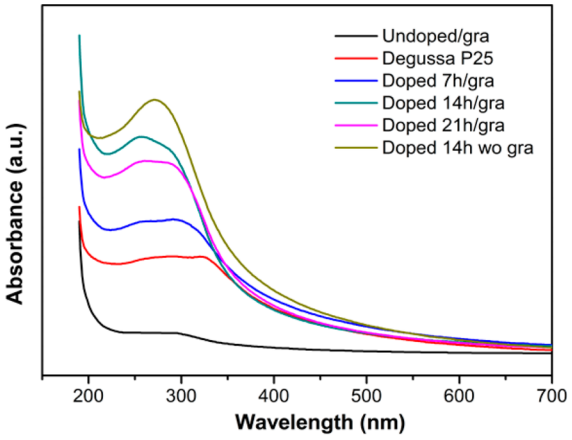

Figure 5. UV−vis absorption spectra of six samples, including undoped TiO_2/graphene, Degussa P25, and N-doped TiO_2/graphene prepared at different doping times of 7, 14, and 21, as well as N-doped TiO_2 without graphene prepared at 14 h.

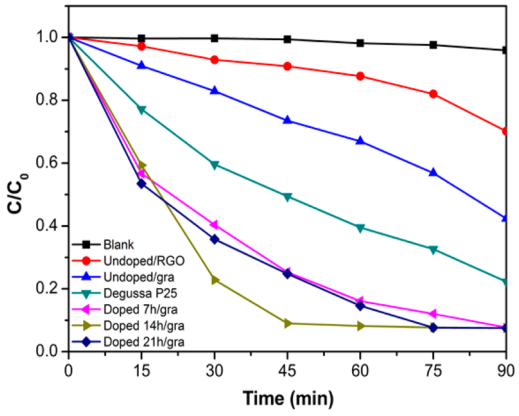

Figure 6. Photodegradation curves of MB on six samples of undoped TiO_2/RGO, undoped TiO_2/graphene, Degussa P25 TiO_2, and N-doped TiO_2/graphene prepared at 7, 14, and 21 h, as well as one blank test.

observed. More specifically, both of our prepared N-doped TiO_2/graphene samples (doped 7 h) and N-doped TiO_2 without graphene (doped 14 h) exhibited better absorption and a certain red shift in the absorption edge, compared with Degussa P25, which suggests that it is more sensitive to visible light. It has been shown that oxygen vacancies give rise to the local states below the conduction band, and the N_i atoms would induce the local states near the valence band edge.[43,58] Therefore, the extension of absorption into the visible range can be definitely attributed to the introduction of N_i dopants and oxygen vacancies in the lattice of the anatase structure, therefore narrowing the bandgap of TiO_2.

To evaluate the potential application of N-doped TiO_2/graphene composites as efficient photocatalysts for pollutant degradation, we conducted the photodegradation curves of MB as a model reaction under visible light. Figure S4 of the Supporting Information is a representative time profile of MB absorbance spectrum with our catalyst (N-doped TiO_2/graphene). These results were compared with measurements of the Degussa P25 TiO_2 under the same conditions. Figure 6 shows time profiles of C/C_0 of MB, where C is the concentration of MB after the specific irradiation time, and C_0 is the concentration of MB in the absorption equilibrium before irradiation. These experimental results indicate that the N-doped TiO_2/graphene composite (doped 14 h) has the best performance among tested samples. Note in Figure 6 that the MB absorption in the 14 h sample drops to the instrument detection limit after 45 min, twice as fast as Degussa P25 TiO_2. We also investigated the degradation curves of undoped TiO_2/RGO and undoped TiO_2/graphene. The results indicated that after irradiation of 90 min, 50% of MB was degraded for the solution containing the undoped TiO_2/graphene sample, while only 30% of MB was degraded for the solution containing the undoped TiO_2/RGO sample. This suggests that photocatalytic performance of undoped TiO_2/graphene is much better than undoped TiO_2/RGO. To confirm the crystalline graphene acting as an acceptor of the photoinduced electrons, we measured the sheet resistance of the exfoliated graphene sheet by a four-probe instrument, as we reported in our previous paper.[26] The resistance was ~850 Ω/sq, at least 3 orders of magnitude less than RGO. Both the photodegradation curves and sheet resistance can prove that the low-defect exfoliated graphene acts as an excellent conductive substrate for electron transfer in comparison with RGO. In addition, we carried out one blank test showing that the solution of MB without TiO_2 was irradiated for 90 min, and only 0.7% of MB degraded.

Furthermore, the durability of the N-doped TiO_2/graphene catalyst was checked for the degradation of MB. The photodegradation of MB was monitored for three consecutive cycles, each lasting 90 min. After each cycle, N-doped TiO_2/graphene was filtered and washed thoroughly with distilled

dx.doi.org/10.1021/sc5001176 | ACS Sustainable Chem. Eng. 2014, 2, 1802−1810

water, and fresh MB solution was added. There was no significant decrease in photodegradation rate during the three consecutive cycles, indicating the good stability of the as-prepared N-doped TiO_2/graphene photocatalyst. We also noted that the pH value of the MB solution plays an important role in the whole photodegradation process. It was found that the decomposition rate of MB increased when the pH values increased, which is likely the result of enhanced adsorption capacity of graphene sheets with more aromatic MB via $\pi-\pi$ conjugation.[12]

In order to quantitatively elucidate the photocatalytic behavior of N-doped TiO_2 clusters, as well as the charge–transfer interaction between TiO_2 and graphene, we have used DFT to compute the electronic structure of N_s- and N_i-doped anatase NCs, both in isolation and contacting a graphene substrate. There are two central concepts to improve the photocatalytic performance of the TiO_2: (1) enabling photo-excitation by visible light and (2) extending the lifetime of the excited state to give holes more time to diffuse to a free surface and form an •OH radical. The former function is achieved by narrowing the TiO_2 band gap by N doping. The purpose of the graphene substrate is to achieve the latter function by separating the electron hole pair but leaving the hole on the TiO_2 to form the radical, as shown in Figure 7. To optimize

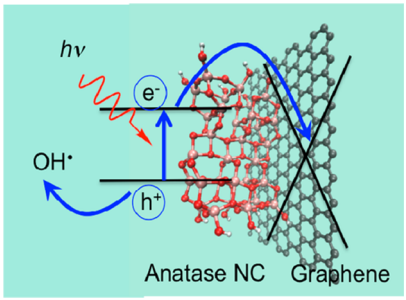

Figure 7. Schematic illustration of the separation of a photoexcited electron hole pair in a TiO_2 NC.

photocatalytic performance the energy of the system is reduced by transferring the photoexcited electron to the graphene, leaving the hole on the TiO_2 where it diffuses to the surface and forms a hydroxyl radical. The horizontal lines over TiO_2 depict the valence and conduction band edges in TiO_2. The crossed lined over the graphene depict the conical band structure of graphene around its Dirac point. As the graphene has no band gap, in order to favor transfer of electrons over holes, the TiO_2 band edges must be shifted up relative to the Dirac point.

The four projected density-of-states (PDOS) plots in left of Figure 8 clearly show that N doping performs as expected to narrow the effective band gap by introducing a doping level. While the TiO_2 NCs are in isolation, the N_i doping and N_s doping give qualitatively different electronic structures. N_s forms a partially filled shallow defect state, while N_i forms a midgap defect state and raises the Fermi energy. These results are in agreement with more accurate DFT+U calculations for N-doped *bulk* anatase with higher doping concentrations and so validate the level of theory used in our calculations.[59] In our calculations, the band structure and Fermi energy of N_s- and N_i-doped particles in isolation differ as shown from the second and third PDOS plots in Figure 8. However, when these differently doped particles are put in contact with graphene, the density of states become very similar—the TiO_2 bands are shifted up relative to the graphene with a shallow defect state at the Fermi energy that narrows the band gap, as shown in the fifth and sixth PDOS plots in Figure 8. The results of these calculations indicate that the photocatalytic potency of the TiO_2-decorated graphene is relatively insensitive to this type of N doping and thus permits the growth of a highly effective photocatalyst at low temperatures.

The PDOS plots in Figure 8 illustrate the band alignment across the TiO_2/graphene heterojunction. It it shown that without N doping the bottom of the TiO_2 conduction band is much closer to the Fermi energy than the top of the TiO_2's valence band, and so energetically, it is more favorable to transfer the hole to graphene rather than the photoexcited electron. Doping TiO_2 with N creates empty states below the graphene Fermi energy. When the N-doped TiO_2 is brought into contact with graphene, these states withdraw 0.8–0.9 electrons from graphene to TiO_2 NCs. This charge transfer in the ground state shifts the TiO_2 bands upward relative to the graphene, pinning the highest occupied electronic state of TiO_2 close to the Fermi energy. This shift in band alignment across the heterojunction makes transfer of the photoexcited electron more favorable.

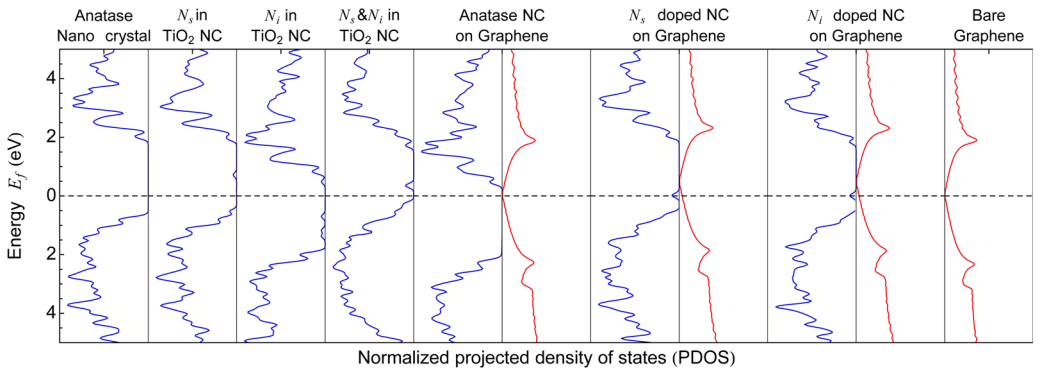

Figure 8. Projected density of electronic states for (from left to right) an undoped TiO_2 NC, N_s-doped TiO_2 NC, N_i-doped TiO_2 NC, TiO_2 NC doped with N_i and N_s, undoped TiO_2/graphene composite, N_s-doped TiO_2/graphene, N_i-doped TiO_2/graphene composite, and graphene in isolation. The blue lines are for states projected onto the TiO_2 NC, and red lines are for states projected onto the graphene. The density of states is plotted relative to a common Fermi energy, indicated by the horizontal dashed lines.

dx.doi.org/10.1021/sc5001176 | *ACS Sustainable Chem. Eng.* 2014, 2, 1802–1810

CONCLUSIONS

In summary, N-doped TiO_2 NCs have been successfully deposited on the surface of exfoliated crystalline graphene by a simple doping process in ammonia solution at a low temperature of 180 °C. Such N-doped TiO_2/graphene composites show excellent photocatalytic efficiency, far exceeding that of commercial Degussa P25. For the composite of graphene-supported N-doped TiO_2, both the conductive carbon platform and the N-doped TiO_2 play synergistic roles during the photodegradation of MB in three ways: (1) enhance the adsorption of aromatic dye on the catalyst via $\pi-\pi$ conjugation between MB and graphene and, therefore, the absorptivity of dyes is better in comparison with Degussa P25, (2) extend light absorption into the visible range by narrowing the bandgap of TiO_2 via N_i-doping, and (3) suppress charge recombination, using crystalline graphene as an acceptor of the photoinduced electrons of the TiO_2 and, therefore, an effective charge separation can be achieved. We believe that the work presented here reveals a new, simple, and scalable strategy for the production of a N-doped TiO_2/graphene composite, which shows great promise for applications as a highly efficient photocatalyst for wastewater purification.

ASSOCIATED CONTENT

Supporting Information

Additional information about TEM images and XRD spectrum of exfoliated graphene, undoped TiO_2/graphene, and N-doped TiO_2/graphene samples; time profile of MB absorbance spectrum; computed PDOS plotted relative to the vacuum level; and a cartoon of the band structure. This material is available free of charge via the Internet at http://pubs.acs.org.

AUTHOR INFORMATION

Corresponding Author

*Email: jiaoj@pdx.edu. Tel: (503) 725-4228. Fax: (503) 725-2815.

Notes

The authors declare no competing financial interest.

ACKNOWLEDGMENTS

This study was supported in part by the National Science Foundation under award numbers ECCS-1057565 and REU-1263339. The computational work was performed using the Extreme Science and Engineering Discovery Environment (XSEDE), which is supported by a National Science Foundation grant, No. OCI-1053575. Electron microscopy was carried out at the Center for Electron Microscopy and Nanofabrication (CEMN), Portland State University, Portland, OR. We acknowledge the National Science Foundation for X-ray diffraction instrumentation (NSF-MRI, award no. DMR-0923572). We also thank Apprenticeships in Science & Engineering intern Abigail M. Lyons for her great help.

REFERENCES

(1) Hoffmann, M. R.; Martin, S. T.; Choi, W. Y.; Bahnemann, D. W. Environmental applications of semiconductor photocatalysis. *Chem. Rev.* **1995**, *95*, 69−96.

(2) Fernandez, A.; Lassaletta, G.; Jimenez, V. M.; Justo, A.; GonzalezElipe, A. R.; Herrmann, J. M.; Tahiri, H.; Aitlchou, Y. Preparation and characterization of TiO_2 photocatalysts supported on various rigid supports (glass, quartz and stainless steel). Comparative studies of photocatalytic activity in water purification. *Appl. Catal., B* **1995**, *7*, 49−63.

(3) Oregan, B.; Gratzel, M. A low-cost, high-efficiency solar-cell based on dye-sensitized colloidal TiO_2 films. *Nature* **1991**, *353*, 737−740.

(4) Asahi, R.; Morikawa, T.; Ohwaki, T.; Aoki, K.; Taga, Y. Visible-light photocatalysis in nitrogen-doped titanium oxides. *Science* **2001**, *293*, 269−271.

(5) Lindgren, T.; Mwabora, J. M.; Avendano, E.; Jonsson, J.; Hoel, A.; Granqvist, C. G.; Lindquist, S. E. Photoelectrochemical and optical properties of nitrogen doped titanium dioxide films prepared by reactive DC magnetron sputtering. *J. Phys. Chem. B* **2003**, *107*, 5709−5716.

(6) Chen, H. Y.; Nambu, A.; Wen, W.; Graciani, J.; Zhong, Z.; Hanson, J. C.; Fujita, E.; Rodriguez, J. A. Reaction of NH_3 with titania: N-doping of the oxide and TiN formation. *J. Phys. Chem. C* **2007**, *111*, 1366−1372.

(7) Burda, C.; Lou, Y. B.; Chen, X. B.; Samia, A. C. S.; Stout, J.; Gole, J. L. Enhanced nitrogen doping in TiO_2 nanoparticles. *Nano Lett.* **2003**, *3*, 1049−1051.

(8) Suda, Y.; Kawasaki, H.; Ueda, T.; Ohshima, T. Preparation of high quality nitrogen doped TiO_2 thin film as a photocatalyst using a pulsed laser deposition method. *Thin Solid Films* **2004**, *453*, 162−166.

(9) Tsetseris, L. Stability and dynamics of carbon and nitrogen dopants in anatase TiO_2: A density functional theory study. *Phys. Rev. B* **2010**, *81*, 165205.

(10) Du, X.; Skachko, I.; Barker, A.; Andrei, E. Y. Approaching ballistic transport in suspended graphene. *Nat. Nanotechnol.* **2008**, *3*, 491−495.

(11) Stankovich, S.; Dikin, D. A.; Dommett, G. H. B.; Kohlhaas, K. M.; Zimney, E. J.; Stach, E. A.; Piner, R. D.; Nguyen, S. T.; Ruoff, R. S. Graphene-based composite materials. *Nature* **2006**, *442*, 282−286.

(12) Zhao, M. F.; Liu, P. Adsorption of methylene blue from aqueous solutions by modified expanded graphite powder. *Desalination* **2009**, *249*, 331−336.

(13) Zhang, H.; Lv, X.; Li, Y.; Wang, Y.; Li, J. P25-graphene composite as a high performance photocatalyst. *ACS Nano* **2010**, *4*, 380−386.

(14) Jiang, G. D.; Lin, Z. F.; Chen, C.; Zhu, L. H.; Chang, Q.; Wang, N.; Wei, W.; Tang, H. Q. TiO_2 nanoparticles assembled on graphene oxide nanosheets with high photocatalytic activity for removal of pollutants. *Carbon* **2011**, *49*, 2693−2701.

(15) Zhou, K.; Zhu, Y.; Yang, X.; Jiang, X.; Li, C. Preparation of graphene−TiO_2 composites with enhanced photocatalytic activity. *New J. Chem.* **2011**, *35*, 353−359.

(16) Liang, Y.; Wang, H.; Casalongue, H. S.; Chen, Z.; Dai, H. TiO_2 nanocrystals grown on graphene as advanced photocatalytic hybrid materials. *Nano Res.* **2010**, *3*, 701−705.

(17) Williams, G.; Seger, B.; Kamt, P. V. TiO_2-graphene nanocomposites. UV-assisted photocatalytic reduction of graphene oxide. *ACS Nano* **2008**, *2*, 1487−1491.

(18) Zhang, Y. H.; Tang, Z. R.; Fu, X.; Xu, Y. J. Engineering the unique 2D mat of graphene to Aachieve graphene-TiO_2 nanocomposite for photocatalytic selective transformation: What advantage does graphene have over its forebear carbon nanotube? *ACS Nano* **2011**, *5*, 7426−7435.

(19) Zhang, Y. H.; Zhang, N.; Tang, Z. R.; Xu, Y. J. Graphene transforms wide band gap ZnS to a visible light photocatalyst. The new role of graphene as a macromolecular photosensitizer. *ACS Nano* **2012**, *6*, 9777−9789.

(20) Zhang, Y. H.; Zhang, N.; Tang, Z. R.; Xu, Y. J. Improving the photocatalytic performance of graphene-TiO_2 nanocomposites via a combined strategy of decreasing defects of graphene and increasing interfacial contact. *Phys. Chem. Chem. Phys.* **2012**, *14*, 9167−9175.

(21) Zhang, N.; Zhang, Y. H.; Xu, Y. J. Recent progress on graphene-based photocatalysts: current status and future perspectives. *Nanoscale* **2012**, *4*, 5792−5813.

(22) Yang, M. Q.; Xu, Y. J. Selective photoredox using graphene-based composite photocatalysts. *Phys. Chem. Chem. Phys.* **2013**, *15*, 19102−19118.

(23) Zhang, Y. H.; Tang, Z. R.; Fu, X. Z.; Xu, Y. J. TiO_2-graphene nanocomposites for gas-phase photocatalytic degradation of volatile aromatic pollutant: Is TiO_2−graphene truly different from other TiO_2−carbon composite materials? *ACS Nano* **2010**, *4*, 7303−7314.
(24) Zhang, N.; Yang, M. Q.; Tang, Z. R.; Xu, Y. J. Toward improving the graphene-semiconductor composite photoactivity via the addition of metal ions as generic interfacial mediator. *ACS Nano* **2014**, *8*, 623−633.
(25) Yin, X.; Zhang, H. L.; Xu, P.; Han, J.; Li, J. Y.; He, M. Simultaneous N-doping of reduced graphene oxide and TiO_2 in the composite for visible light photodegradation of methylene blue with enhanced performance. *RSC Adv.* **2013**, *3*, 18474−18481.
(26) Qian, W.; Chen, Z.; Cottingham, S.; Merrill, W. A.; Swartz, N. A.; Goforth, A. M.; Clare, T. L.; Jiao, J. Surfactant-free hybridization of transition metal oxide nanoparticles with conductive graphene for high-performance supercapacitor. *Green Chem.* **2012**, *14*, 371−377.
(27) Qian, W.; Hao, R.; Zhou, J.; Eastman, M.; Manhat, B. A.; Sun, Q.; Goforth, A. M.; Jiao, J. Exfoliated graphene-supported Pt and Pt-based alloys as electrocatalysts for direct methanol fuel cells. *Carbon* **2013**, *52*, 595−604.
(28) Qian, W.; Cottingham, S.; Jiao, J. Hybridization of conductive few-layer graphene with well-dispersed Pd nanocrystals. *Appl. Surf. Sci.* **2013**, *275*, 342−346.
(29) Hummers, W. S.; Offeman, R. E. Preparation of graphitic oxide. *J. Am. Chem. Soc.* **1958**, *80*, 1339−1339.
(30) Zhang, C. Z.; Hao, R.; Liao, H. B.; Hou, Y. L. Synthesis of amino-functionalized graphene as metal-free catalyst and exploration of the roles of various nitrogen states in oxygen reduction reaction. *Nano Energy* **2013**, *2*, 88−97.
(31) Marcano, D. C.; Kosynkin, D. V.; Berlin, J. M.; Sinitskii, A.; Sun, Z. Z.; Slesarev, A.; Alemany, L. B.; Lu, W.; Tour, J. M. Improved synthesis of graphene oxide. *ACS Nano* **2010**, *4*, 4806−4814.
(32) Soler, J. M.; Artacho, E.; Gale, J. D.; Garcia, A.; Junquera, J.; Ordejon, P.; Sanchez-Portal, D. The SIESTA method for ab initio order-N materials simulation. *J. Phys.-Condes. Matter* **2002**, *14*, 2745−2779.
(33) Wu, Z. G.; Cohen, R. E. More accurate generalized gradient approximation for solids. *Phys. Rev. B* **2006**, *73*.
(34) Yang, H. G.; Sun, C. H.; Qiao, S. Z.; Zou, J.; Liu, G.; Smith, S. C.; Cheng, H. M.; Lu, G. Q. Anatase TiO_2 single crystals with a large percentage of reactive facets. *Nature* **2008**, *453*, 638−641.
(35) Diebold, U. The surface science of titanium dioxide. *Surf. Sci. Rep.* **2003**, *48*, 53−229.
(36) Tsetseris, L. Configurations, electronic properties, and diffusion of carbon and nitrogen dopants in rutile TiO_2: A density functional theory study. *Phys. Rev. B* **2011**, *84*, 165201.
(37) Zambelli, T.; Trost, J.; Wintterlin, J.; Ertl, G. Diffusion and atomic hopping of N atoms on Ru(0001) studied by scanning tunneling microscopy. *Phys. Rev. Lett.* **1996**, *76*, 795−798.
(38) Cong, Y.; Zhang, J.; Chen, F.; Anpo, M. Synthesis and characterization of nitrogen-doped TiO2 nanophotocatalyst with high visible light activity. *J. Phys. Chem. C* **2007**, *111*, 6976−6982.
(39) Chen, X. B.; Burda, C. Photoelectron spectroscopic investigation of nitrogen-doped titania nanoparticles. *J. Phys. Chem. B* **2004**, *108*, 15446−15449.
(40) Prokes, S. M.; Gole, J. L.; Chen, X.; Burda, C.; Carlos, W. E. Defect-related optical behavior in surface-modified TiO_2 nanostructures. *Adv. Funct. Mater.* **2005**, *15*, 161−167.
(41) Gyorgy, E.; del Pino, A. P.; Serra, P.; Morenza, J. L. Depth profiling characterisation of the surface layer obtained by pulsed Nd: YAG laser irradiation of titanium in nitrogen. *Surf. Coat. Technol.* **2003**, *173*, 265−270.
(42) Yang, X. X.; Cao, C. D.; Erickson, L.; Hohn, K.; Maghirang, R.; Klabunde, K. Synthesis of visible-light-active TiO_2-based photocatalysts by carbon and nitrogen doping. *J. Catal.* **2008**, *260*, 128−133.
(43) Diwald, O.; Thompson, T. L.; Zubkov, T.; Goralski, E. G.; Walck, S. D.; Yates, J. T. Photochemical activity of nitrogen-doped rutile TiO_2 (110) in visible light. *J. Phys. Chem. B* **2004**, *108*, 6004−6008.
(44) Liu, G.; Wang, X. W.; Wang, L. Z.; Chen, Z. G.; Li, F.; Lu, G. Q.; Cheng, H. M. The role of crystal phase in determining photocatalytic activity of nitrogen doped TiO_2. *J. Colloid Interface Sci.* **2009**, *334*, 171−175.
(45) Li, D.; Haneda, H.; Hishita, S.; Ohashi, N. Visible-light-driven N-F-codoped TiO_2 photocatalysts. 2. Optical characterization, photocatalysis, and potential application to air purification. *Chem. Mater.* **2005**, *17*, 2596−2602.
(46) Li, F. B.; Li, X. Z. The enhancement of photodegradation efficiency using Pt-TiO_2 catalyst. *Chemosphere* **2002**, *48*, 1103−1111.
(47) Zhang, J. L.; Hu, Y.; Matsuoka, M.; Yamashita, H.; Minagawa, M.; Hidaka, H.; Anpo, M. Relationship between the local structures of titanium oxide photocatalysts and their reactivities in the decomposition of NO. *J. Phys. Chem. B* **2001**, *105*, 8395−8398.
(48) Liu, G.; Wang, X. W.; Chen, Z. G.; Cheng, H. M.; Lu, G. Q. The role of crystal phase in determining photocatalytic activity of nitrogen doped TiO_2. *J. Colloid Interface Sci.* **2009**, *329*, 331−338.
(49) Yoon, M.; Seo, M.; Jeong, C.; Jang, J. H.; Jeon, K. S. Synthesis of liposome-templated titania nanodisks: Optical properties and photocatalytic activities. *Chem. Mater.* **2005**, *17*, 6069−6079.
(50) Wan, Q.; Wang, T. H.; Zhao, J. C. Enhanced photocatalytic activity of ZnO nanotetrapods. *Appl. Phys. Lett.* **2005**, *87*, 083105.
(51) Wang, E. J.; He, T.; Zhao, L. S.; Chen, Y. M.; Cao, Y. A. Improved visible light photocatalytic activity of titania doped with tin and nitrogen. *J. Mater. Chem.* **2011**, *21*, 144−150.
(52) Tang, H.; Prasad, K.; Sanjines, R.; Schmid, P. E.; Levy, F. Electrical and optical-properties of TiO_2 anatase thin-films. *J. Appl. Phys.* **1994**, *75*, 2042−2047.
(53) Pillai, S. C.; Periyat, P.; George, R.; McCormack, D. E.; Seery, M. K.; Hayden, H.; Colreavy, J.; Corr, D.; Hinder, S. J. Synthesis of high-temperature stable anatase TiO_2 photocatalyst. *J. Phys. Chem. C* **2007**, *111*, 1605−1611.
(54) Berger, H.; Tang, H.; Levy, F. Growth and raman-spectroscopic characterization of TiO_2 anatase single-crystals. *J. Cryst. Growth* **1993**, *130*, 108−112.
(55) Ferrari, A. C.; Meyer, J. C.; Scardaci, V.; Casiraghi, C.; Lazzeri, M.; Mauri, F.; Piscanec, S.; Jiang, D.; Novoselov, K. S.; Roth, S.; Geim, A. K. Raman spectrum of graphene and graphene layers. *Phys. Rev. Lett.* **2006**, *97*, 187401.
(56) Ferrari, A. C. Raman spectroscopy of graphene and graphite: Disorder, electron-phonon coupling, doping and nonadiabatic effects. *Solid State Commun.* **2007**, *143*, 47−57.
(57) Graf, D.; Molitor, F.; Ensslin, K.; Stampfer, C.; Jungen, A.; Hierold, C.; Wirtz, L. Spatially resolved raman spectroscopy of single- and few-layer graphene. *Nano Lett.* **2007**, *7*, 238−242.
(58) Prokes, S. M.; Gole, J. L.; Chen, X. B.; Burda, C.; Carlos, W. E. Defect-related optical behavior in surface-modified TiO_2 nanostructures. *Adv. Funct. Mater.* **2005**, *15*, 161−167.
(59) Zhao, Z.; Liu, Q. Mechanism of higher photocatalytic activity of anatase TiO_2 doped with nitrogen under visible-light irradiation from density functional theory calculation. *J. Phys. D: Appl. Phys.* **2008**, *41*, 025105.